Bulgarian Chemical Communications, Volume 55, Special Issue A (pp. 119-125) 2023 DOI: 10.34049/bcc.55.A.0019

Strontium-doped lanthanum nickelate ($LaNiO_3$) nano-materials for alkaline water splitting

P. Mishra[1], P. Sharma[1], V. Singh[2], N. K. Singh[1*]

[1]*Department of Chemistry, Faculty of Science, University of Lucknow, Lucknow-226007, India*
[2]*Department of Chemistry, Maharana Pratap Govt. P.G. College, Hardoi, U.P. India, Pin code- 241001*

Received: April 25, 2023; Revised: August 7, 2023

Innovative perovskite-type oxides, specifically $La_{1-x}Sr_xNiO_3$ (where $0 \leq x \leq 0.8$), were skillfully synthesized using a low-temperature citric acid sol-gel approach. These novel materials were then subjected to comprehensive scrutiny to explore their remarkable electrocatalytic potential in the context of alkaline water splitting. Characterizations were performed by using oxide material as anode at which oxygen evolution reaction (OER) takes place. Through X-ray diffraction (XRD) examination, it was unveiled that the material was predominantly composed of an almost pure phase. Delving into the cyclic voltammogram (CV) data, a mesmerizing duo of redox peaks emerged, one anodic and its counterpart cathodic, observed just before starting of OER within the potential range of 0-0.7V in 1 M KOH solution at room temperature. The research brought to light a remarkable boost in electrocatalytic activity upon Sr substitution for La in $LaNiO_3$. Additionally, an intriguing discovery unfolded, showing a unity order for the OER concerning shifts in OH^- concentration, accompanied by Tafel slopes spanning the fascinating range of 85 to 101 mV $decade^{-1}$. The lower values of electrochemical activation energy ($\Delta E^{o}_{el}{}^{\#}$) and highly negative values of entropy of activation ($\Delta S^{o\#}$) favor a high rate of electrochemical formation of oxygen, which arises through adsorption phenomenon.

Keywords: XRD, Perovskite; Sol-gel; Water splitting; Tafel plot; Electrocatalytic activity

INTRODUCTION

Transition metals (Mn, Fe, Co, Ni) mixed oxides with perovskite type structure are important electrode materials for various applications such as efficient oxygen anode in water electrolysis [1-5] and as a cathode in solid oxide fuel cells and metal air batteries [6-8]. The major problems associated with electrocatalytic activity of the electrode for OER were the higher potential value and deterioration of electrode materials. It was further observed that electrocatalytic efficiency towards OER decreases with cell operation due to formation of a very thin resistant layer of NiO over the nickel electrode [9, 10]. In order to reduce internal resistance several suitable membranes, *viz*., reinforced asbestos, sintered nickel, PTFF bonded zirconia, nickel net backed porous cermets membrane, etc., have been developed. Nickel is unstable and not suitable for the anodic polarization conditions. So, work is continued to reduce the oxygen overpotential with low-cost electrode material. For the purpose, investigations were carried out to obtain economical electrode materials by powder coating [11], raney nickel coating [12], electrodeposition [13, 14], plasma spraying [15] methods to improve the porosity and hence the surface area of the nickel electrodes. Several other materials have also been investigated for oxygen evolution reaction other than nickel. Transition metals oxides with spinel (e.g. Co_3O_4 and $NiFe_2O_4$) and perovskite (e.g. $La_{1-x}Sr_xCoO_3$, $La_{1-x}Sr_xNiO_3$, $La_{1-x}Sr_xMnO_3$, etc.) structure, their cost-effectiveness, widespread accessibility, and remarkable resistance to corrosion in alkaline media, are setting them apart as a distinguished choice in the scientific community [16]. In the dawn of research, conventional ceramic and thermal decomposition methods reigned supreme for the synthesis of these materials at elevated temperatures [17-19]. Conventional methods in earlier studies yielded oxides with larger particle sizes and lower specific surface areas, while recent low-temperature synthetic approaches utilizing solid organic precursors have shown promising results in producing oxides with significantly enhanced specific surface areas [20-23]. Through the implementation of advanced low-temperature synthesis techniques and the utilization of organic precursors, scientists effectively created Sr-substituted perovskite materials. These pioneering substances demonstrated a remarkable improvement in electrocatalytic performance, surpassing those generated through conventional high-temperature ceramic and thermal decomposition methodologies. In a recent seminal research endeavor, Lal *et al*. [24] embarked on a comprehensive exploration of the electrochemical behavior governing the oxygen evolution reaction (OER) in $La_{1-x}Sr_xCoO_3$ materials,

* To whom all correspondence should be sent:
E-mail: nksbhu@yahoo.com singh_narendra@lkouniv.ac.in

where x ranged from 0 to 0.4. Notably, these intriguing specimens were meticulously synthesized using the sophisticated stearic acid sol-gel method. Furthermore, the team diligently investigated the physicochemical attributes of these compounds, employing state-of-the-art techniques. The investigation uncovered a striking resemblance between the roughness aspect of the oxide surface and the evident electrocatalytic behavior in both the Sr-substituted lanthanum cobaltites and the Sr-substituted lanthanum manganite. The latter was produced using the sol-gel technique, employing malic acid and polyacrylic acid.

The interfacial and electrocatalytic properties of these materials are widely recognized to be significantly influenced by various preparation variables. These include the concentration of the starting substances, pH of the solution, temperature, method of preparation, characteristics of precursors, and ionic substitution. Given the mentioned considerations, we meticulously examined the electrocatalytic behavior of copper-substituted lanthanum cobaltites, which was synthesized *via* sol-gel technique in acidic medium [25]. Encouragingly, our findings unveiled favorable outcomes in terms of its performance towards the oxygen evolution reaction (OER).

MATERIALS AND METHODS

Chemical and reagents

All the chemicals used were either AR-grade or purified grade, so, no further purification has been done. Perovskite-type oxides of La, Sr and Ni having composition $La_{1-x}Sr_xNiO_3$ ($0 \leq X \leq 0.8$), were synthesized by adopting the low-temperature citric acid sol-gel method reported by Vassiliou *et al*. [26]. In this method, metal nitrates, citric acid and ethylene glycol were mixed together in double distilled water in appropriate proportions. Gel formation was catalyzed by the addition of few drops of HNO_3. The excess nitric acid was boiled off and the gel so obtained was heated on a hot plate till the gel burnt out completely into solid mass with evolution of brown fumes. The solid was then crushed into fine powder and further annealed at 650 °C for 6 hours in a muffle furnace (ASCO) to get the desired material.

Equipments and measurements

The presence of a single perovskite phase in the prepared oxides was confidently ascertained by capturing X-ray diffraction patterns with the XPERT-PRO diffractometer (Model PW3050/60) employing a Cu-Kα (λ = 1.54048 Å) radiation source. To determine the crystallite size, Scherrer's formula was diligently utilized. Furthermore, the texture of the oxide in its powder form underwent thorough examination through scanning electron microscopy (JEOL JSM 6490LV). For the precise execution of cyclic voltammogram (CV) and Tafel experiments, we employed the advanced capabilities of an electrochemical workstation, the Gamry Reference 600 ZRA. This workstation is equipped with a potentiostat/galvanostat and specialized corrosion & physical electrochemistry software, facilitating accurate control and comprehensive measurements throughout the entire electrochemical testing procedure. Throughout the experiment, we harnessed the power of three exceptional electrodes: a platinum foil (serving as the auxiliary electrode, boasting an area of ~2 cm^2), Hg/HgO/1M KOH (taking on the role of the reference electrode, showcasing an electrode potential of E° = 0.098 V *vs* NHE at 25°C), and an oxide film on Ni-support (our working electrode, expertly prepared following well-established literature procedures [27, 28]). To ensure seamless connections and minimize the iR drop, we seamlessly integrated a Luggin capillary, infused with gel prepared by mixing agar-agar and potassium chloride in a definite stoichiometry, into the electrochemical cell. This ingenious setup ensured a precision-driven measurement experience and empowered full control throughout the captivating electrochemical journey.

RESULTS AND DISCUSSION

X-ray diffraction (XRD)

Intriguing X-ray diffraction patterns (XRD) of $LaNiO_3$ and $La_{0.2}Sr_{0.8}NiO_3$ were explored from 20° to 100° (Figure 1). Astonishingly close matches to JCPDS ASTM file 25-1060 and COD ID 1000308 confirmed their exceptional crystallinity. In our extensive investigation, we have made captivating discoveries concerning the diffraction patterns of $LaNiO_3$ and $La_{0.2}Sr_{0.8}NiO_3$. Notably, the CA-SG method showcased its remarkable efficiency, producing materials with near-pure perovskite phases, highlighting its exceptional capabilities. To delve deeper into their characteristics, we employed Scherer's formula [$S = \frac{0.9\,\lambda}{B\,\mathrm{Cos}\theta}$] [29] to calculate the crystallite size, yielding fascinating results. $LaNiO_3$ exhibited an impressive crystallite size of approximately 25 nm, while $La_{0.2}Sr_{0.8}NiO_3$ displayed a slightly smaller size, measuring around 18 nm. The obtained X-ray diffraction patterns for $LaNiO_3$were subjected to Rietveld refinement using Full Prof suite to calculate accurate unit cell dimensions. From the refined data the crystals were found to be of hexagonal structure with space group R -3 c and cell parameters a = b = 5.46, c = 13.19; α=β=90°,γ=120°.

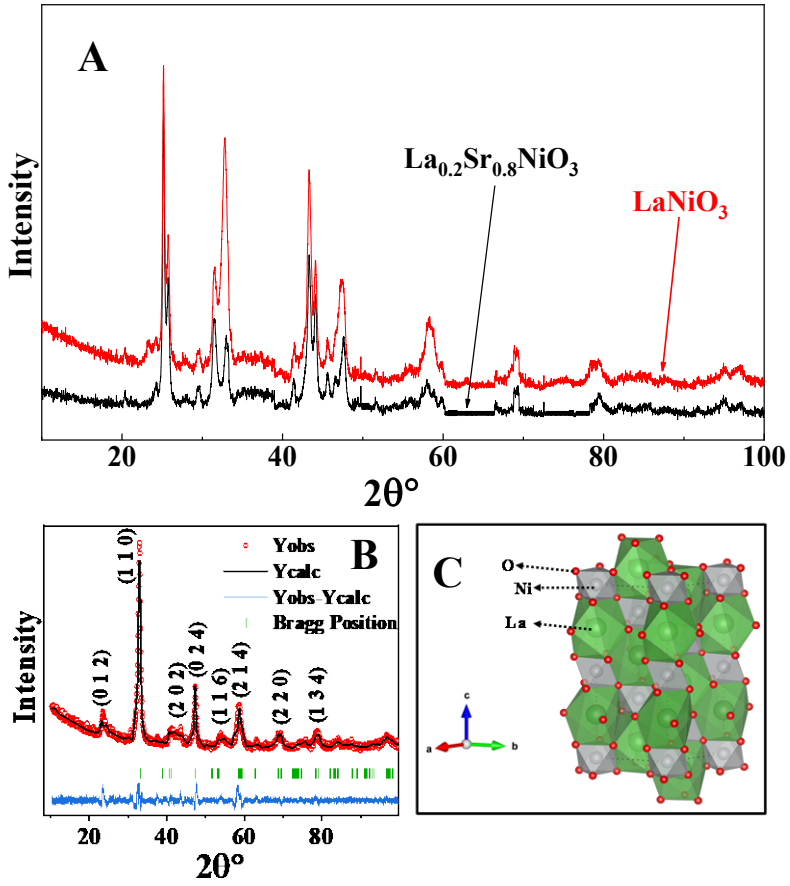

Figure 1 (A). XRD powder patterns of $LaNiO_3$; **(B)** Refined XRD profile of $LaNiO_3$; **(C)** Crystal structure of $LaNiO_3$

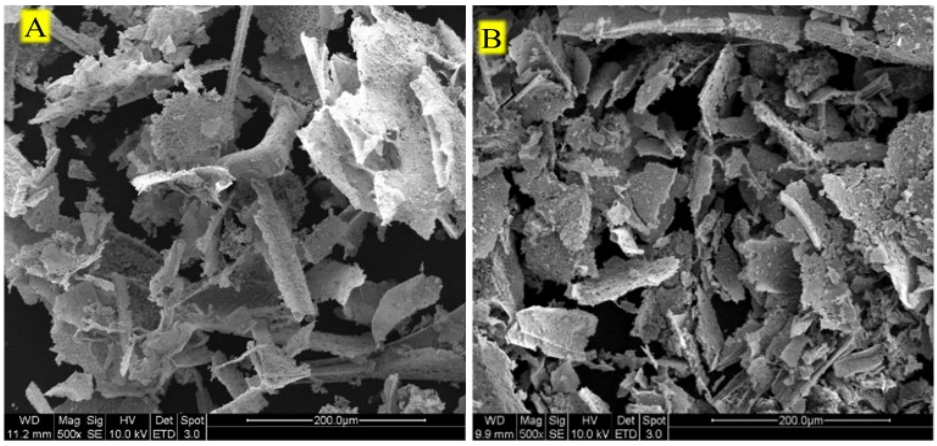

Figure 2. SE micrographs of **(A)** $LaNO_3$; **(B)** $La_{0.2}Sr_{0.8}NiO_3$ oxide powder sintered at 650°C for 6 h.

Table 1. Values of the cyclic voltammetric parameters of $Ni/La_{1-x}Sr_xNiO_3$ ($0 \leq x \leq 0.8$) in 1 M KOH at 25°C (scan rate = 20 $mVsec^{-1}$)

Electrode Materials	E_{Pa} (mV)	E_{Pc} (mV)	ΔE_P (mV)	$E°=(E_{Pa}+E_{Pc})/2$ /mV	j_{pa} (mA cm^{-2})	j_{pc} (mA cm^{-2})	$\frac{j_{pa}}{j_{pc}}$	Q (mC cm^{-2})
$LaNiO_3$	475	382	93	428	0.66	0.33	2.0	5.8
$La_{0.8}Sr_{0.2}NiO_3$	481	382	99	431	0.65	0.40	1.6	8.7
$La_{0.5}Sr_{0.5}NiO_3$	478	381	95	430	0.94	0.57	1.6	11.3
$La_{0.2}Sr_{0.8}NiO_3$	482	398	84	440	1.16	0.96	1.2	23.6

The quality factors of the refined profile are in an acceptable range with χ^2 value = 2.4926 for $LaNiO_3$.

Scanning electron micrography (SEM)

Figure 2 shows the SE micrographs of the materials annealed at 650°C for 5 h at magnification ×500. Materials represented a flake-like structure with slightly small size for $La_{0.2}Sr_{0.8}NiO_3$, which shows better performance in the splitting of alkaline water.

Cyclic voltammetry (CV)

Behold Figure 3(A), presenting a mesmerizing cyclic voltammogram of the exquisite electrocatalyst film electrodes gracing the surface of Ni. With grace and precision, this enchanting data was measured at a scan rate of 20 mV/sec, exploring the captivating potential region of 0.0 - 0.7 V. Bathed in the brilliance of a 1 M KOH solution at a serene 25°C. Observe each voltammogram, adorned with a delightful set of redox peaks, just before the fascinating event of water splitting takes place. The corresponding redox peak potentials were found to vary with 478 ± 4 and 390 ± 8, respectively. Singh *et al.* [27] has also observed similar redox peaks with $LaNiO_3$ oxide electrode. According to their research, the captivating redox peaks arise from the process of gaining or losing electrons in the Ni. The formal redox potential was calculated by averaging the positive and negative potential which are almost similar with each oxide electrode. Other voltammetric parameters such as anodic & cathodic peak potential difference (ΔE_P), anodic (j_{p_a}) & cathodic (j_{p_c}) maximum current and total charge (q) obtained from the integrated CV curve are tabulated in Table 1. The enchanting value of j_{p_a}/j_{p_c}, surpasses unity, hinting at the captivating irreversibility of the redox couple. Behold, the values of the esteemed cyclic voltammetric parameters proudly grace Table 1, revealing their mystical secrets. It is noteworthy that the significant increase in charge with Sr-substitution for La in the oxide matrix leads to the improvement in catalytic activity for OER. Maximum charge value (~4 times) was observed with 0.8 mol Sr-substitution. Delving into the allure of the experiment, we ventured to study the impact of scan rate on the CV parameters. With fervor and precision, we meticulously recorded CV curves across a range of 20-120 mV sec^{-1} in the enchanting realm of 1M KOH at STP (25°C). The voltammogram for $La_{0.2}Sr_{0.8}NiO_3$ is given in Figure 3(B). With each step of our study, a bewitching transformation unfolded: the anodic peak potentials (23-37 mV) shifted towards higher potentials, while the cathodic peak potentials (7-22 mV) drifted towards lower potentials. This mesmerizing phenomenon emerged as we increased the scan rate, promising to reveal enthralling insights into the system's dynamics. The shifting in potential indicates the irreversible [27, 28] process of electron transfer. The integrated voltammetric charge (q) was obtained by combining the positive and negative segments of the curve, up to just preceding the onset of the OER. With exception to $La_{0.2}Sr_{0.8}NiO_3$, the value of charge was found to decrease with increase of scan rate. The voltammetric charge (q) against $(\text{scan rate})^{-1/2}$ shows direct relation (Figure 3(C)) which indicates diffusion of species-controlled formation of redox couple at oxide/electrode interface [28, 30].

Electrocatalytic activity

The alluring world of electrocatalytic activity unfolded before our eyes as we meticulously recorded iR-compensated anodic Tafel experiments (E *vs* log j) (Figure 3(D)). This captivating endeavor took place at a leisurely scan rate of 0.2 mV/sec, immersed in 1M KOH solution at a serene 25°C. The catalyst represents similar nature in the curves regardless of the substitution of Sr for La in the $LaNiO_3$ lattice. For Tafel slope, we focused on initial linear section of the curve and observed that the Tafel slope value decreased with Sr-substitution except $La_{0.8}Sr_{0.2}NiO_3$ oxide. Among the oxide electrode tested, the oxide with 0.8 Sr-substitution was found to be the most active electrode towards water splitting. Gathering insights from the data relating to current density at 800 mV, a mesmerizing revelation takes shape, unveiling the distinctive order of electrocatalytic activity among the diverse oxide electrodes $La_{0.2}Sr_{0.8}NiO_3$ (j= 25.2mAcm^{-2}) > $La_{0.5}Sr_{0.5}NiO_3$ (j= 4.4mAcm^{-2})> $La_{0.8}Sr_{0.2}NiO_3$ (j=3.4 mAcm^{-2}) > $LaNiO_3$ (j= 1.9 mAcm^{-2}). It is noteworthy that the Tafel slopes (85-101 mV decade^{-1}) observed with the oxide catalysts were almost similar to those reported in literature particularly for $La_{0.8}Sr_{0.2}MnO_3$ (108 mV decade^{-1}), $La_{0.6}Sr_{0.4}MnO_3$ (108 mVdecade^{-1}), $La_{0.6}Sr_{0.4}MnO_3$ (103 mVdecade^{-1}) and $La_{0.7}Sr_{0.3}MnO_3$ (92 mVdecade^{-1}) obtained by malic acid [20], citric acid [21], polyacrylic acid [22], citric acid-ethylene diamine [23] and $La_{0.6}Cu_{0.4}CoO_3$ [25] sol-gel routes, respectively. Although these oxides have similar Tafel slope values yet have better electrocatalytic activity towards OER as compared to oxides reported in the present work. But, $La_{0.7}Sr_{0.3}MnO_3$ synthesized by auto combustion technique [31] (j = 2 mA cm^{-2} at 750 mV in 1M LiOH) has lower electrocatalytic property. Unveiling the order required a captivating pursuit, leading us to record the anodic polarization curve

(Figure 3(E) for $La_{0.2}Sr_{0.8}NiO_3$) across various KOH concentrations. Throughout the experiment, we ensured the uniformity of electrical intensity for each electrolytic solution. To achieve this objective, we fixed the ionic strength of 1.5 for each electrolyte by introducing KNO_3.The enchanting curve provided us with a wealth of current density data (log j in A cm^{-2}) at a specific potential. This mesmerizing data was then plotted against log [OH^-], creating the captivating Figure 3(F). The inclination of the line divulged an almost unity slope value for the order of reaction in every instance (Table 2). The enthralling Tafel slopes and order of the OER listed in Table 2, suggest the compelling proposition: the OER occurring at the electrocatalysts goes on with the similar mechanism.

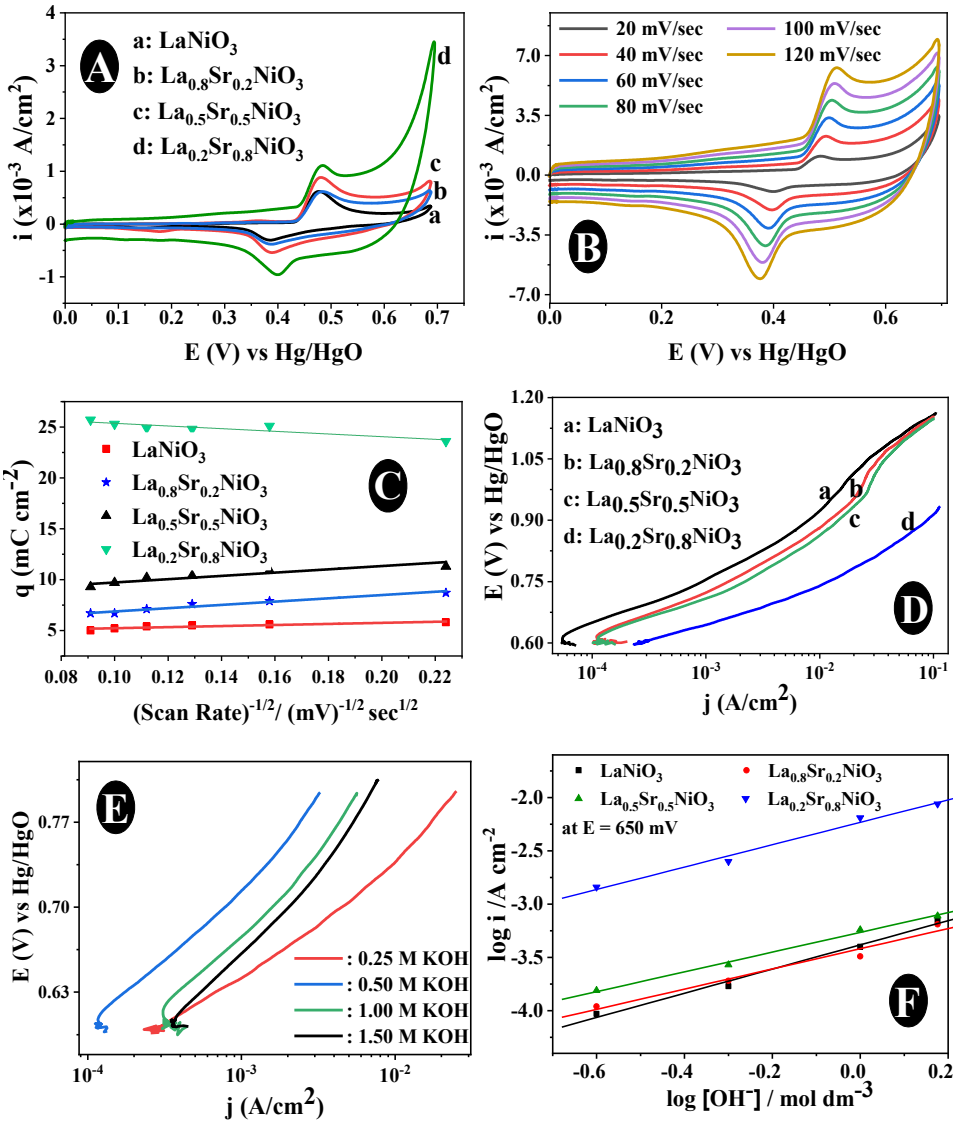

Figure 3. (A) Cyclic voltammograms of Ni/$La_{1-x}Sr_xNiO_3$ ($0 \le x \le 0.8$) film electrode at 20 mV sec^{-1} scan rates in 1M KOH (25°C); **(B)** CV of Ni/$La_{0.2}Sr_{0.8}NiO_3$ film electrode at different scan rates in 1M KOH (25 °C); **(C)** Plot of voltametric charge (q) *vs* (scan rate)$^{-1/2}$ for the oxide film electrode on Ni; **(D)** Anodic polarization curve for Ni/$La_{1-x}Sr_xNiO_3$ ($0 \le x \le 0.8$) in 1M KOH (25°C); SR: 0.2 mVsec^{-1}; **(E)** Tafel curves of Ni/$La_{0.2}Sr_{0.8}NiO_3$ in different KOH concentrations (μ = 1.5) at 25°C; **(F)** Plot of log j *vs* log [OH^-] for the oxide electrode at 25°C

Table 2. Electrode kinetic parameters for oxygen evolution reaction on $Ni/La_{1-x}Sr_xNiO_3$ ($0 \le x \le 0.8$) in 1 M KOH at 25 ˚C

Electrode	Tafel slope / mVd^{-1}	Order (p)	E/ mV at j ($mA\ cm^{-2}$)		j ($mA\ cm^{-2}$) at E / mV		
			10	100	700	750	800
$LaNiO_3$	95	1.2	926	1162	0.3	0.9	1.9
$La_{0.8}Sr_{0.2}NiO_3$	101	0.9	885	1159	0.6	1.5	3.4
$La_{0.5}Sr_{0.5}NiO_3$	89	0.9	867	1150	0.8	2.0	4.4
$La_{0.2}Sr_{0.8}NiO_3$	85	1.0	740	916	4.0	11.5	25.2

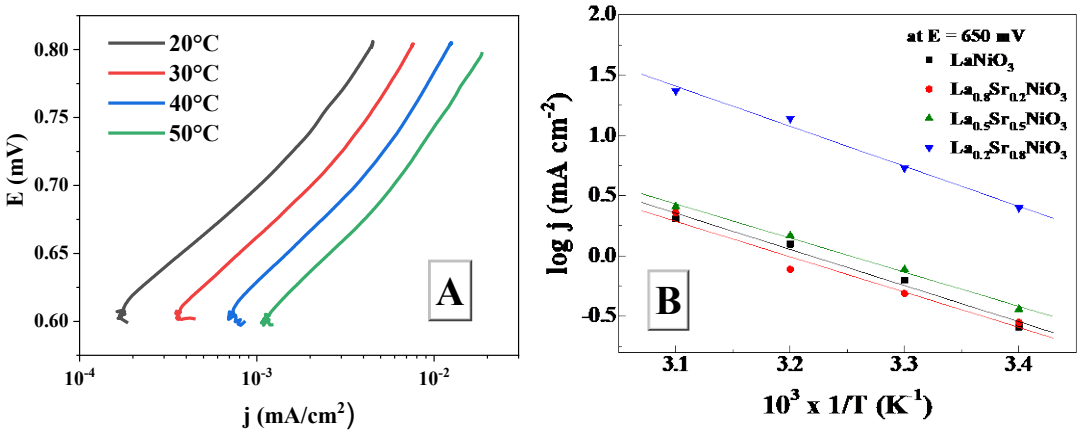

Figure 4. (A) Anodic polarization curve for the oxide film electrodes, $La_{0.2}Sr_{0.8}NiO_3$, at different temperatures; **(B)** Arrhenius plot for the oxide electrode at a constant applied potential (650 mV) in 1 M KOH

Table 3. Thermodynamic parameters for O_2 evolution on $Ni/La_{1-x}Sr_xNiO_3$ ($0 \le x \le 0.8$) in 1 M KOH

Electrode	$\Delta H_{el}^{\circ\neq}$ ($KJ\ mol^{-1}$) at E = 650 mV	$-\Delta S^{\circ\neq}$ ($J\ deg^{-1}\ mol^{-1}$)	α	$\Delta H^{\circ\neq}$ ($KJ\ mol^{-1}$)
$LaNiO_3$	36.9	227.4	0.6	57.7
$La_{0.8}Sr_{0.2}NiO_3$	36.9	227.4	0.6	57.7
$La_{0.5}Sr_{0.5}NiO_3$	34.5	233.5	0.5	51.5
$La_{0.2}Sr_{0.8}NiO_3$	39.6	199.5	0.6	61.0

Thermodynamic study

Embarking on a captivating journey into thermodynamic parameters, we recorded anodic polarization in 1M KOH at varying temperatures. Witness the enchanting Figure 4(A), featuring a set of mesmerizing polarization curves at 20, 30, 40, and 50°C for $La_{0.2}Sr_{0.8}NiO_3$ at unwaveringly maintained steadfast temperature for the reference electrode. From the captivating Arrhenius plot, log j vs 1/T (Figure 4(B)), at a specific potential of 650 mV, we derived the standard apparent enthalpy of activation ($\Delta H_{el}^{\circ\#}$). This mesmerizing parameter was skillfully evaluated inclination of the plots. The value of log j (in $mA\ cm^{-2}$) was diligently deduced from the curve, meticulously measured at varying temperatures. Furthermore, by using relations (1) and (2) [32, 33] more thermodynamic parameter was investigated:

$$\Delta H_{el}^{\circ\#} = \Delta H^{\circ\#} - \alpha F \quad (1)$$

$$\Delta S^{\circ\#} = 2.3R\ [\log j + \Delta H_{el}^{\circ\#}/2.3RT - \log(nF\omega C_{OH^-})] \quad (2)$$

The terms mentioned in relation (1) and (2) have their general meanings. The transfer coefficient (α) was determined by using the relation 2.303RT/bF. In this captivating pursuit, the gas constant (R), Faraday constant (F), Tafel slope ('b') in mV $decade^{-1}$ and overpotential (η) [34], absolute temperature (T) played pivotal roles. Within the realm of equation (2), an enthralling frequency factor ω (= k_BT/h) emerges, with k_B and h signifying the universal constants. Embarking on meticulous calculations, we derived the values of these captivating thermodynamic parameters, tabulated in the illustrious Table 3. From the table, it is observed that each oxide electrode has almost similar value of activation energy. The emergence of a profoundly negative value for $\Delta S^{\circ\#}$ holds captivating implications, pointing to the intriguing involvement

of captivating interactions during the oxygen evolution reaction.

CONCLUSION

The captivating findings from this research work unveil the profound influence of Sr substitution in the base oxide ($LaNiO_3$) on both its physicochemical and electrocatalytic properties. The oxide, $La_{0.2}Sr_{0.8}NiO_3$, boasts an astonishing 12-fold increase in catalytic power compared to $LaNiO_3$ in the realm of alkaline water splitting. Additionally, the XRD data showcases nearly pure phases of the oxide materials, adding to their enchanting allure.

Acknowledgement: *The authors express their sincere appreciation to the Department of Chemistry, University of Lucknow for the essentials and laboratory and to Birbal Sahni Institute of Palaeosciences, Lucknow for conducting the SEM analyses. The Council of Science and Technology, U.P. is also been acknowledged for the financial support by a Research Project (ID: 1720).*

REFERENCES

1. Y. Matsumoto, E. Sato, *Electrochim. Acta*, **24,** 421 (1979).
2. Y. Matsumoto, S. Yamada, T. Nishida, E. Sato, *J. Electrochem. Soc.,* **127**, 2360 (1980).
3. S. Yamada, Y. Matsumoto, E. Sato, *J. Electrochem. Soc. Jpn.,***49**, 269 (1981).
4. B. JO'M, T. Otagawa, Young, *J. Electroanal. Chem. Interfacial Electrochem.,* **150** 633 (1983).
5. S. Tiwari, P. Chartier and R. N. Singh, *J. Electrochem. Soc.,***142,** 148 (1995).
6. D. Meadowcroft, *Nature,* **226,** 847 (1970).
7. Y. Shimizu, H. Matsuda, N. Miura, N. Yamazoe, *Chem. Lett.,* **21**, 1033 (1992).
8. J. Suntivich, H. A. Gasteiger, N. Yabuuchi, H. Nakanishi, J. B. Goodenough, Y. Shao-Horn, *Nat. Chem.,***3,** 546 (2011).
9. J. Chang, Y. Xiao, M. Xiao, J. Ge, C. Liu, W. Xing, *ACS Catal.,***5**, 6874 (2015).
10. S. Jin, *Acs Energy Letters*, **2,** 1937 (2017).
11. D. E. Hall, *J. Electrochem. Soc.*, C41 (1985).
12. L. Chen, A. Lasia, *J. Electrochem. Soc.*, **138,** 3321 (1991).
13. J. De Carvalho, G. Tremiliosi Filho, L. A. Avaca, E. Gonzalez, *International Journal of Hydrogen Energy*,**14,** 161 (1989).
14. Y. Ogata, H. Hori, M. Yasuda, F. Hine, *J Electrochem. Soc,*, **135,** 76 (1988).
15. D. E. Hall, *J Appl Electrochem*, 107 (1984).
16. K. Zeng, X. Zheng, C. Li, J. Yan, J. H. Tian, C. Jin, P. Strasser, R. Yang, *Adv. Funct. Mater.,***30**, 2000503 (2020).
17. J. O. M. Bockris, T. Otagawa, *J. Electrochem. Soc.,***131**, 290 (1984).
18. J. Balej, *Int. J. Hydrogen Energy,***10**, 89 (1985).
19. A. Kobussen, F. Van Buren, T. Van den Belt, H. Van Wees, *J. Electroanal. Chem.,***115**, 131 (1980).
20. N. K. Singh, S. Tiwari, R. N. Singh, *Int. J. Hydrogen Energy*, **23,** 775 (1998).
21. T. Sharma, N. K. Singh, S.K. Tiwari, R. N. Singh, *Ind. J. Eng. Mat. Sci*., **5**, 38 (1998)
22. N. K. Singh, B. Lal, R. N. Singh, *Int. J. Hydrogen Energy,***27**, 885 (2002).
23. B. Lal, N. K. Singh, R. N. Singh, *Indian J. Chem.,***40A***,* 1269 (2001).
24. B. Lal, M. Raghunandan, M. Gupta, R. N. Singh, *Int. J. Hydrogen Energy,* **30**, 723 (2005).
25. N. K. Singh, M. Yadav, C. Fernandez, *Int. J. Electrochem. Sci.,***12**, 7128 (2017).
26. J. K. Vassiliou, M. Hornbostel, R. Ziebarth, F. J. Disalvo, *J. Solid State Chem.,***81**, 208 (1989).
27. R. N. Singh, S. Tiwari, S. Singh, A. Jain, N. K. Singh, *Int. J. Hydrogen Energy,* **22**, 557 (1997).
28. R. N. Singh, S. K. Tiwari, S. P. Singh, N. K. Singh, G. Poillerat, P. Chartier, *J. Chem. Soc. Faraday Trans.,***92**, 2593 (1996).
29. N. Fradette, B. Marsan, *J. Electrochem. Soc.,***145**, 2320 (1998).
30. N. K. Singh, P. Sharma, M. K. Yadav, R. Parihar, *Int. J. Electrochem. Sci.,***15**, 7001 (2020).
31. B. Shin, S. Choi, Y. Tak, *Int. J. Electrochem. Sci,* 5900 (2016).
32. N. K. Singh, P. Sharma, I. Kumar, A. S. Chaddha, *Int. J. Electrochem. Sci*, **14,** 11379 (2019).
33. E. Gileadi, Electrode Kinetics, VCH Publishers Inc, New York, USA, 1993, p. 151.
34. R. N. Singh, J. Pandey, N. K. Singh, B. Lal, P. Chartier, J.-F. Koenig, *Electrochim. Acta*, **45,** 1911 (2000).